

# A comprehensive quality control algorithm for atmospheric motion vectors and its impacts on analysis and forecast of the China Meteorological Administration Global Forecast System

Jincheng Wang<sup>1,2,3</sup> | Jie Feng<sup>4,5,6</sup> | Yi Yang<sup>2,7</sup> | Jianglin Hu<sup>1,3</sup> | Junli Yang<sup>1,3</sup>

<sup>1</sup>CMA Earth System Modeling and Prediction Center, China Meteorological Administration, Beijing, China

<sup>2</sup>School of Atmospheric Sciences, Lanzhou University, Lanzhou, China

<sup>3</sup>State Key Laboratory of Severe Weather, Chinese Academy of Meteorological Sciences, Beijing, China

<sup>4</sup>Department of Atmospheric and Oceanic Sciences, Institute of Atmospheric Sciences, Fudan University, Shanghai, China

<sup>5</sup>Shanghai Key Laboratory of Ocean-Land-Atmosphere Boundary Dynamics and Climate Change, Fudan University, Shanghai, China

<sup>6</sup>Shanghai Academy of Artificial Intelligence for Science, Shanghai, China

<sup>7</sup>Key Laboratory of Climate Resource Development and Disaster Prevention in Gansu Province, Lanzhou, China

## Correspondence

Yi Yang, School of Atmospheric Sciences, Lanzhou University, Lanzhou, China.  
 Email: [yangyi@lzu.edu.cn](mailto:yangyi@lzu.edu.cn)

## Funding information

National Natural Science Foundation of China, Grant/Award Numbers: 12241103, 42375150

## Abstract

Atmospheric motion vector (AMV) data play a crucial role in improving the forecast skills of models. Quality control is an essential step that affects the assimilation effectiveness of the AMVs. In a bid to rectify the deviation issue of the initial (analysis) atmospheric dynamic field in the troposphere and to improve AMV assimilation and the forecast skill of the China Meteorological Administration Global Forecast System (CMA-GFS), a comprehensive quality control (CQC) method is proposed in this study. The CQC encompasses a quality indicator check and blacklist establishment for the AMVs, as well as the background field check based on biweight statistics in the bivector space. Detailed analysis of AMV data eliminated by CQC steps reveals its effectiveness in excluding high and low wind speed outliers, normalizing the probability density function (PDF) of observation-minus-background ( $O - B$ ) values to a Gaussian distribution, thus resolving leptokurtic and platykurtic distribution issues. A 35-day assimilation sensitivity experiment shows that the original quality control (OQC) increases analysis and forecast errors, especially in tropical wind fields by over 10%. In contrast, CQC significantly reduces these errors, with an average tropospheric dynamic field error decrease of over 3% in the Southern Hemisphere. The CQC's biweight method in bivector space demonstrates potential for quality control of atmospheric dynamic field observations.

## KEY WORDS

4DVAR, atmospheric motion vectors, biweight quality control method, data assimilation

## 1 | INTRODUCTION

Atmospheric motion vectors (AMVs), obtained by tracking clouds or water vapour characteristics in consecutive satellite images (Nieman et al., 1997), represent crucial

wind field observations for the data assimilation systems of global medium-range weather prediction models. The AMV data play a key role in improving the accuracy of initial and forecast fields of global numerical weather prediction (NWP), particularly in enhancing the accuracy

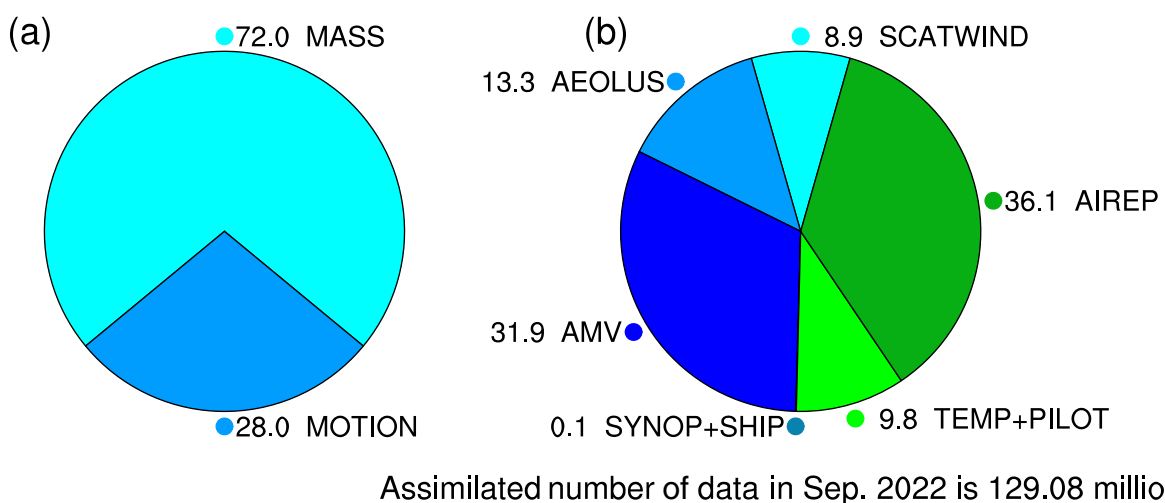


**FIGURE 1** Proportions (%) of (a) mass field and dynamic field data, and (b) different dynamic field data types assimilated in the four-dimensional variational data assimilation (4DVAR) system of the China Meteorological Administration Global Forecast System (CMA-GFS) in September, 2022. The total number of assimilated observations is 129.08 million pieces. [Colour figure can be viewed at [wileyonlinelibrary.com](http://wileyonlinelibrary.com)]

of tropical and Southern Hemisphere mean wind fields (Bormann et al., 2012). In current operational global data assimilation (DA) systems, most of assimilated observations are mass field data associated with temperature and humidity such as the remote-sensing observations from satellites. However, the dynamic field observational data associated with wind for the assimilation are obviously insufficient, especially in the oceanic, tropical and Southern Hemisphere regions. For example, in the four-dimensional variational assimilation (4DVAR) system of the China Meteorological Administration (CMA)-Global Forecast System (GFS), the assimilated wind field observations account for only 28% of the total (Figure 1a).

At present, the assimilated dynamic field observations in global NWP models consist of wind data from radiosondes (TEMP), small pilot balloons (PILOT), ground-based synoptic weather stations (SYNOP), ships, the Aeolus satellite, ocean observations, aircraft reports (AIREP) and the AMVs (Figure 1b). Among them, the AMV and AIREP data are relatively abundant, accounting for 31.9% and 36.1% of the total wind field data in the CMA-GFS 4DVAR system, respectively. In the above wind field observations, only AMV, AIREP, TEMP, PILOT and Aeolus observations can depict the three-dimensional (3D) characteristics of wind fields. The TEMP and PILOT data are mainly obtained from few stations on land, with only two observations per day (0000 UTC and 1200 UTC) and low spatio-temporal resolution. The AIREP can provide sufficient vertical wind profile data over land airports and upper-level wind fields around 200 hPa along air routes and over the ocean surface in the Northern Hemisphere.

The Aeolus satellite, launched successfully in August 2018, provides abundant and high-quality vertical wind profile data worldwide, which substantially improve the accuracy of the analysis fields and forecast skill of global NWP models in the troposphere over tropical and polar regions (Martin et al., 2023; Rennie et al., 2021). The AMVs are the main source of 3D wind observations over oceans and the Southern Hemisphere. The global meteorological satellite observation system, composed of several polar-orbiting satellites and geostationary satellites, can provide 3D wind field observations with temporal resolutions from 30 min to 12 hours. These observations cover the tropics, the Southern Hemisphere and polar regions, thus making a major contribution to improving the analysis and forecast accuracy for atmospheric circulations (Baker et al., 2022). There is a consensus that more 3D atmospheric wind observation data are necessary for both the NWP operational requirements and scientific research (Stoffelen et al., 2020). Nevertheless, in April 2023, the Aeolus satellite was decommissioned. Pending the launch of new Aeolus satellites or other satellites, AMV data have become an important supplement for the 3D wind observation data over oceans and in the Southern Hemisphere to maintain the relatively stable proportion of assimilated wind field observations in global medium-range NWP models.

Various studies have demonstrated that the accuracy of the initial and forecasted dynamic fields for global medium-range NWP models over the Southern Hemisphere and oceans can be improved through assimilating new wind profile data (such as the wind profile data from the Aeolus satellite) or enhancing the application strategy for the current operational AMV assimilation

(Bormann et al., 2019; Lee et al., 2022; Martin et al., 2023; Rennie et al., 2021). The latter approach is more economical. There are two major factors affecting the effectiveness of AMV assimilation. One is the error characteristics of AMV data. Although the retrieval algorithms for the AMVs are relatively mature and share similar principles, which mainly include feature tracking and vertical profiling, the specific technical details for calculating the AMVs vary among different satellite operation centres (Sanek et al., 2019; Xu et al., 2002). Additionally, there are differences in calibration accuracy and vertical profiling among different satellites, which lead to variations in the error characteristics of the AMVs (Bormann et al., 2003; Cordoba et al., 2017; Sanek et al., 2019). The other factor is the quality control of AMV data. Due to the variable quality of the AMVs from different satellites, all the global medium-range NWP centres have carried out meticulous quality control on AMV data before assimilation (Bormann et al., 2012), to ensure the assimilation of more high-quality wind field data.

For the calculation of the AMVs, every satellite operation centre meticulously examines the data quality (Deb et al., 2020; Holmlund, 1998; Holmlund et al., 2001; Nieman et al., 1997; Xu et al., 2002) and assigns a quality indicator (QI) to each data point to characterize its reliability. In general, a smaller QI represents poorer data quality, while a QI of 100 signifies the best data quality. However, the methods and thresholds for assigning the QI to the AMVs vary among different satellite operation centres. Due to the differences in AMV retrieval algorithms and the definition methods and thresholds of the QI (Holmlund et al., 2001; Xu et al., 2002), the same QI value may represent different data uncertainties. QI for the AMVs serves as a crucial index for quality control before

assimilation, and more stringent quality control for the AMVs is also required to perform global medium-range NWP (Bormann et al., 2012; Wang et al., 2022). There are three main aspects of AMV quality control methods. The first uses the QI to conduct quality control to eliminate the AMV data with a QI less than a certain threshold value. The second is the establishment of a blacklist. The AMV blacklist is developed by long-term monitoring and statistical evaluation of each AMV type. Different NWP centres adopt different blacklist systems, such as the European Centre for Medium-Range Weather Forecasts Integrated Forecast System<sup>1</sup> and the UK Met Office system.<sup>2</sup> The other one is background field checks, whereby data are excluded if the deviation from the background field (observation minus background, O – B) exceeds a certain multiple of the sum of observation and background errors. The quality control method for the AMVs in the CMA-GFS system (a global medium-range NWP model developed by the CMA Earth System Modeling and Prediction Center) is shown in Table 1. It can be summarized as adopting the same QI threshold for all AMV data types, and the blacklist including only data at altitudes below 975 hPa and above 150 hPa, as well as AMV data retrieved from water vapour channels and mixed channels.

The verification and assessment of the CMA-GFS 4DVAR scheme indicates that the analysis field of velocity potential at 200 hPa (Figure 2b) shows positive deviations compared with that of ERA5 (Figure 2a) over the western tropical Pacific Ocean, eastern Indian Ocean and southern North America, and exhibits negative deviations over the eastern tropical Pacific Ocean (Figure 2c). The results of an AMV denial experiment (AMV\_DENY) without AMV assimilation demonstrate that the velocity potential function analysis field at 200 hPa (Figure 2d) does not

**TABLE 1** Original quality control scheme and comprehensive quality control scheme proposed in this study for the atmospheric motion vector (AMV) data in the four-dimensional variational data assimilation (4DVAR) system of the China Meteorological Administration Global Forecast System (CMA-GFS).

Rejected criteria		
Steps of quality control	OQC	CQC
Blacklist	1. Wind derived from water vapour channels, multispectral channels, clear-sky water vapour channels, ozone channels 2. All the AMVs at altitudes below 975 hPa and above 150 hPa	See details in Table 2
QI	QI < 80.0	QI < 80.0
Background check	$ O - B  > 5.0\sigma_o$	Biweight background check in bivector space ( $Z_i^{O-B_w} > 3.0, Z_i^{O-B_d} > 3.0, Z_i^{O-B_u} > 3.0, \text{ or } Z_i^{O-B_v} > 3.0$ )

Note: QI indicates the quality indicator, and O – B denotes observation-minus-background errors.

Abbreviations: CQC, comprehensive quality control; QI, quality indicator; O – B, observation minus background; OQC, original quality control.

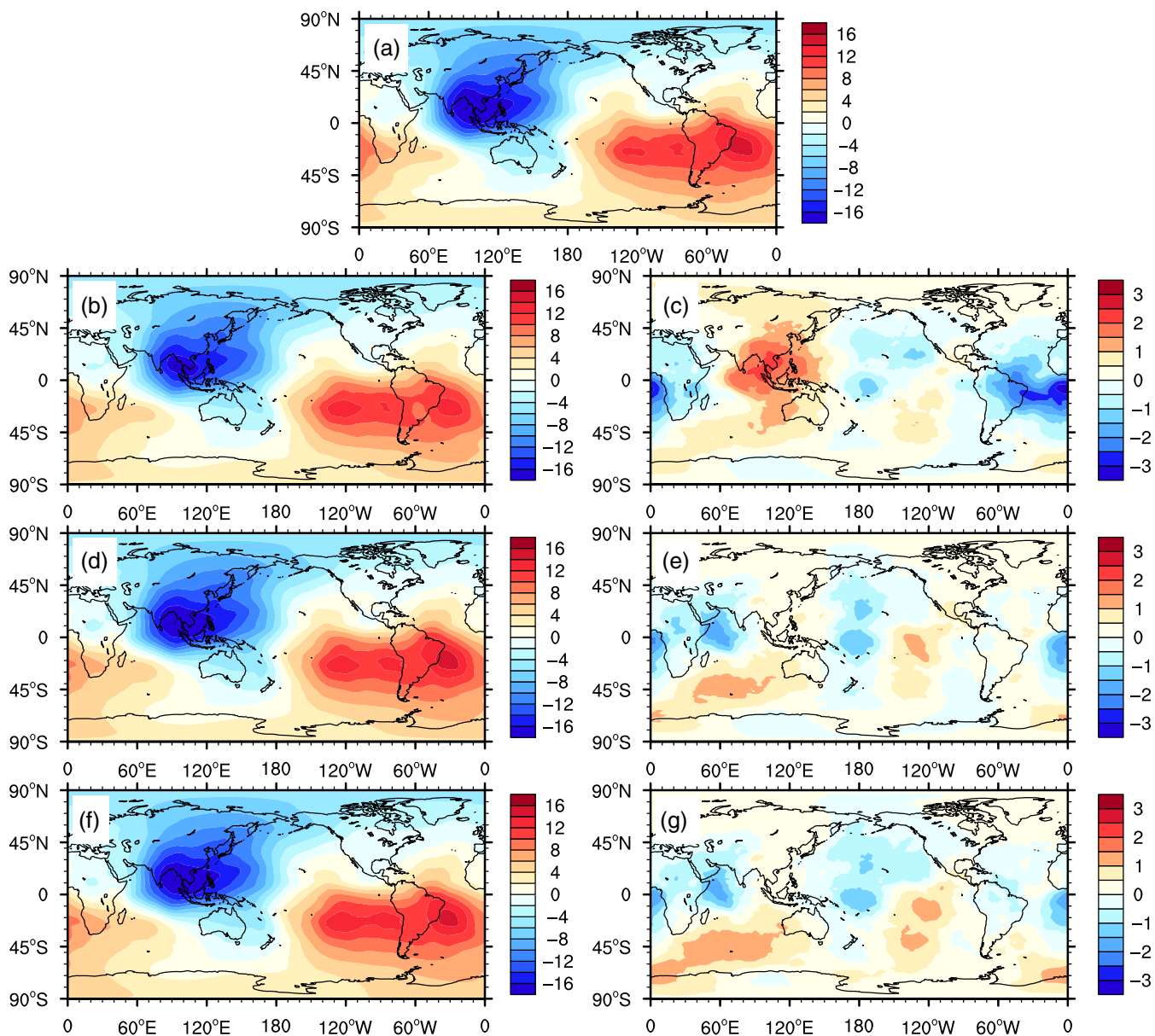


**FIGURE 2** Mean velocity potential functions ( $10^6 \text{ m}^2 \cdot \text{s}$ ) at 200 hPa from 1200 UTC 15 August to 1200 UTC 15 September 2022 from: (a) the fifth-generation European Centre for Medium-Range Weather Forecasts atmospheric reanalysis data (ERA5); (b) the analysis field of the China Meteorological Administration Global Forecast System (CMA-GFS) operational system (AMV\_OQC); (d) the analysis field of the experiment without AMV assimilation (AMV\_DENY); and (f) the analysis field after the comprehensive quality control (CQC) in the CMA-GFS (AMV\_CQC), and the differences in the mean velocity potential functions from (c) the AMV\_OQC (AMV\_OQC – ERA5); (e) AMV\_DENY (AMV\_DENY – ERA5); and (g) AMV\_CQC (AMV\_CQC – ERA5) relative to the ERA5. [Colour figure can be viewed at [wileyonlinelibrary.com](http://wileyonlinelibrary.com)]

have obvious systematic deviations in the tropic regions (Figure 2e), indicating that the deviations in the velocity potential field are caused by improper assimilation of the AMVs. Additionally, the root-mean-squared errors (RMSEs) of u- and v-wind analysis fields in the CMA-GFS 4DVAR system increase by more than 30% compared with the results of the AMV-DENY (as shown in Section 3.2). However, all previous studies and evaluations have shown that the assimilation of AMV data has made markedly

positive contributions to the global medium-range NWP (Bormann et al., 2012; Wang et al., 2022). Therefore, the obvious deviations of the analysis field of velocity potential function in the CMA-GFS system are caused by the defects of the quality control method, which needs to be improved urgently. To address this issue, we propose a comprehensive quality control (CQC) algorithm for the AMVs in this study, which adopts the AMV blacklist and background check based on the biweight method in the bivector

space of wind speed, wind direction and easterly–westerly wind ( $u$  component) and northerly–southerly wind ( $v$  component).

The remainder of this paper is organized as follows. Section 2 analyzes the shortcomings of the AMV quality control method in the CMA-GFS in detail and introduces the CQC method for the AMVs. In addition, the statistical characteristics of the original, eliminated and retained observation data after quality control are also analyzed. In Section 3, based on the CMA-GFS assimilation prediction system, numerical experiments are carried out to analyze and compare the influences of the CQC method on the analysis and forecast fields. The main conclusions are summarized in Section 4.

## 2 | QUALITY CONTROL FOR THE AMVS

### 2.1 | Original quality control method in the CMA-GFS 4DVAR operational system

The original quality control (OQC) method for the AMVs used in the CMA-GFS 4DVAR operational system version 3.4 (V3.4) consists of three steps (Table 1). Firstly, the AMVs with a QI value less than 80 ( $QI < 80$ ) are discarded.

Secondly, the AMV data derived from water vapour channels, multispectral channels, clear-sky water vapour channels and ozone channels are excluded, along with the AMV data at altitudes below 975 hPa and above 150 hPa. Finally, background field checks are conducted to eliminate the data with an  $O - B$  value larger than five times the observation error. Note that all AMVs are thinned in 200 km by 200 km by 50 hPa boxes and then thinned AMVs are assimilated into CMA-GFS 4DVAR.

The probability density distribution (PDF) of  $O - B$  values after the OQC is shown in Figure 3a,b. In terms of  $u$  wind, the  $O - B$  values are  $-0.10 \text{ m}\cdot\text{s}^{-1}$  on average, showing a skewed distribution with the skewness of  $-0.31$ . The peak value of the PDF is higher, with a kurtosis of 4.12. Note that the kurtosis values in this study have been subtracted from the kurtosis value (3.0) of the standard normal distribution. For  $v$  wind, the  $O - B$  values are  $-0.03 \text{ m}\cdot\text{s}^{-1}$  on average, and the peak value of the PDF is also higher, with a kurtosis of 2.95. The above results indicate that after the OQC, the frequency within both the central section ( $|OMB| < 1 \text{ K}$ ) and the two end sections ( $|OMB| > 3 \text{ K}$ ) is higher than the frequency of Gaussian distribution determined by the mean value and the standard deviation of the samples. The PDFs of the  $O - B$  values of  $u$  and  $v$  wind after the OQC display a leptokurtic distribution (a probability distribution that has a higher

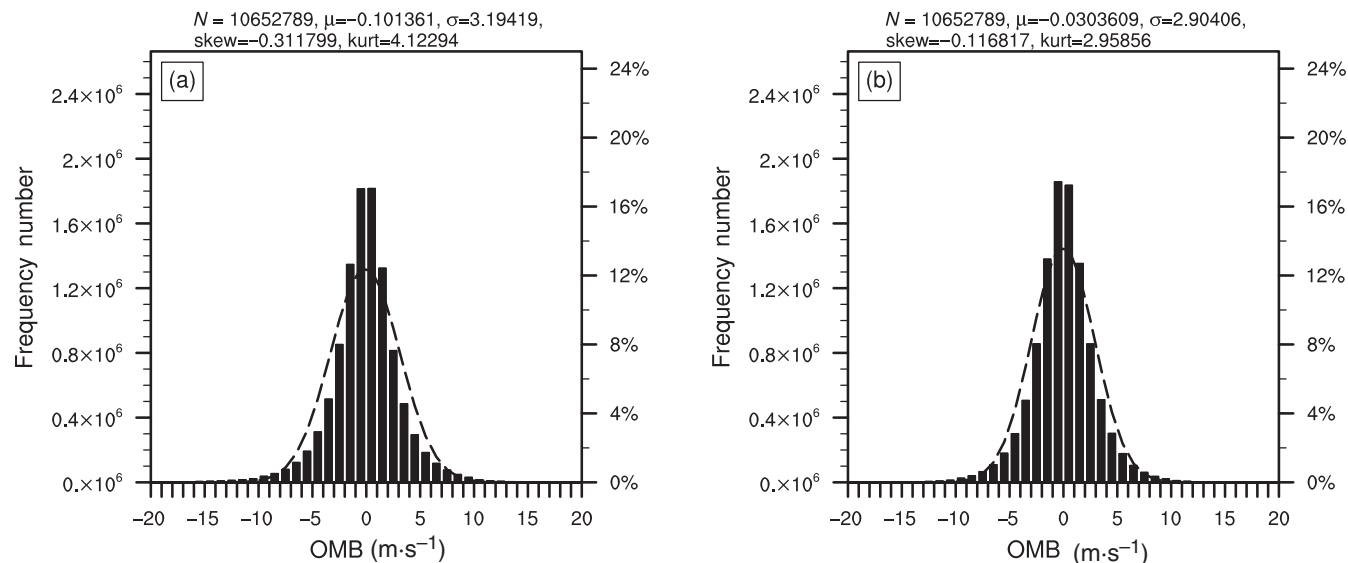


**FIGURE 3** Frequencies (histograms) and Gaussian probability density functions (PDFs) (black lines) of the observation-minus-background errors ( $O - B$ ) of the (a)  $u$  and (b)  $v$  wind assimilated in the AMV\_OQC from 0300 UTC on 15 August to 2100 UTC on 15 September 2022.  $N$  is the number of observations,  $\mu$  and  $\sigma$  are the mean and standard deviation. ‘Skew’ and ‘kurt’ represent skewness and kurtosis values respectively. The skewness is a statistical measure of the asymmetry of the probability distribution, where a value of zero indicates symmetric distribution, and a negative (positive) value means asymmetric distribution with flatter left (right) tail distribution. The kurtosis is a statistical measure that describes the shape of a distribution’s tails in relation to its peak: a value of zero means the distributions have tails and a peak comparable to a normal distribution, and a positive (negative) value means heavier (lighter) tails and a sharper (flatter) peak compared to a normal distribution.

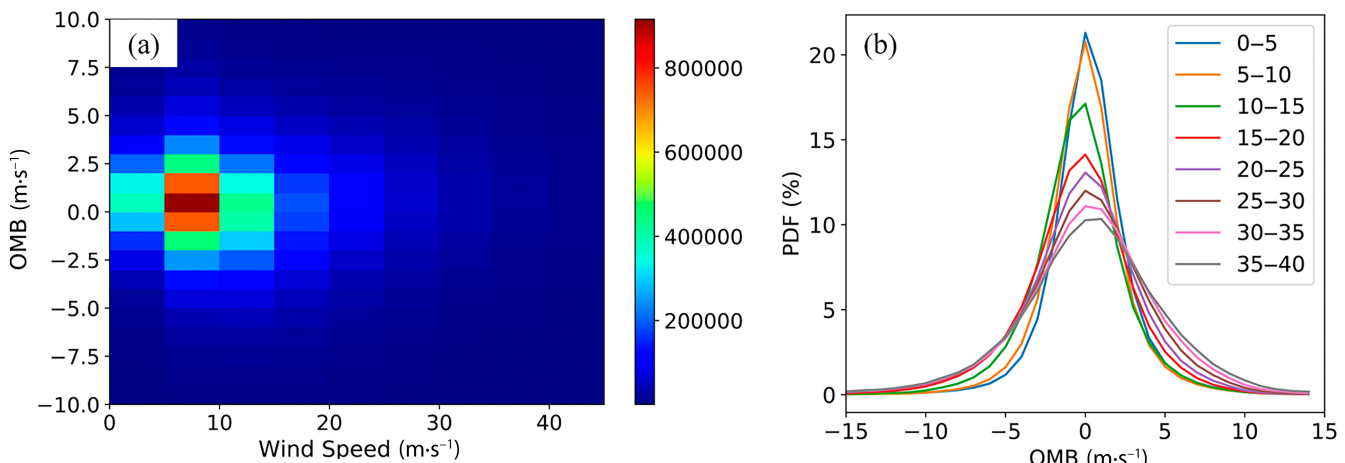


**FIGURE 4** (a) Frequencies (colours) and (b) probability density functions (PDFs) of the O – B of u wind after the OQC from 0300 UTC on 15 August to 2100 UTC on 15 September 2022. Different colours in Figure 4b represent different wind speed ranges. The data samples have been sparsified. [Colour figure can be viewed at [wileyonlinelibrary.com](http://wileyonlinelibrary.com)]

kurtosis than a normal distribution) and a platykurtic distribution (a probability distribution that has flatter peaks and thinner tails compared to a normal distribution), which is quite different from the unbiased Gaussian distribution and thus cannot meet the hypothetical condition of an unbiased Gaussian distribution for O – B in the variational assimilation system (Lorenc, 1986). Further analysis reveals that after the OQC, the lower absolute O – B values of u wind are concentrated in the low wind speed section ( $<10\text{ m}\cdot\text{s}^{-1}$ ), as shown in Figure 4a. The O – B PDFs of u wind under different wind speed conditions (Figure 4b) demonstrate that after the OQC, the leptokurtic distribution is mainly caused by low wind speed ( $<10\text{ m}\cdot\text{s}^{-1}$ ) and the platykurtic distribution is mainly related to high wind speed ( $>20\text{ m}\cdot\text{s}^{-1}$ ).

Compared with the results from experiment AMV\_DENY, we can find that after assimilating the AMV data subjected to the OQC in the CMA-GFS 4DVAR system, the errors of u- and v-wind analysis fields relative to ERA5 increase by more than 30% (as shown in Section 3.2). This result means that assimilating the AMV data after the OQC has an obvious negative contribution to the model analysis field. Moreover, assimilating the AMV data after the OQC leads to pronounced positive deviations of the velocity potential function at 200 hPa over the western tropical Pacific Ocean and the eastern Indian Ocean, and prominent negative deviations over the tropical Atlantic (Figure 2c). There is no systematic bias in experiment AMV\_DENY (Figure 2e). These results contradict the consensus from previous studies indicating positive contributions of assimilating AMV data to the global NWP. The negative contribution of AMV assimilation is related

to the poor quality control for the AMVs in the CMA-GFS 4DVAR.

## 2.2 | Comprehensive quality control method in bivector space

In order to improve the AMV assimilation in the CMA-GFS 4DVAR system and solve the problem of the leptokurtic and platykurtic distribution of the AMV O – B values after the OQC, we propose the CQC method for the AMVs in bivector space in this study. The detailed steps of the quality control scheme are as follows:

1. **Blacklist.** According to the statistical results of the mean values and standard deviations of the AMV O – B values from each satellite instrument and channel for at least one month, the data with an O – B mean value greater than  $1\text{ m}\cdot\text{s}^{-1}$  are added to the blacklist, as shown in Table 2.
2. **QI quality control.** Removing the u- and v-wind data with  $\text{QI} < 80$ .
3. **Biweight background check in bivector space.** The primary goal of quality control is to eliminate outliers from observations. A common approach is to estimate the mean and standard deviation of a variable and then exclude the data that deviate from the mean by several times the standard deviation. However, traditional estimates of mean value and standard deviation are sometimes severely distorted by the presence of some outliers, which makes it extremely difficult to identify outliers. For this reason, the biweight method

TABLE 2 Blacklist of the comprehensive quality control (CQC) for the atmospheric motion vectors (AMVs).

Satellites	AMV data types	Altitudes	Latitudes
All	All	150 hPa or 975 hPa	All
All	3, 4, 5, 6, 7	All	All
FY-2G	1	850–500 hPa, 650–100 hPa	All
FY-2H	1	850–600 hPa, 500–100 hPa	All
INSAT-3D	1	1000–700 hPa, 450–100 hPa	All
INSAT-3DR	1	1000–700 hPa, 450–100 hPa	All
Excluding GOES-16, Himawari-8 and Himawari-9	2	All	All
Himawari-8, Himawari-9	All	850–550 hPa	25° S–25° N
GOES-16,17	All	1000–300 hPa	25° S–25° N
METEOSAT-11	All	1000–450 hPa, 200–100 hPa	25° S–25° N

Note: 1, the AMVs from infrared channels; 2, the AMVs from the visible channels; 3, the AMVs from water vapour channels; 4, the AMVs from a combination of spectral channels; 5, the AMVs from clear-sky water vapour channels; 6, the AMVs from ozone channels; and 7, the AMVs from water vapour channel (cloud or clear-sky condition not specified).

(Lanzante, 1996) is used to estimate the mean and standard deviation, which are minimally influenced by the outliers. Currently, the biweight method is widely used for the quality control of satellite and occultation data (Nie et al., 2022; Zou & Zeng, 2006), yielding excellent results.

In the vector space of wind speed and direction and the vector space of u wind and v wind, the biweight quality control of the O–B of wind speed, wind direction, u wind and v wind is carried out. The Z-scores of the O–B of wind speed ( $Z_i^{O-B_w}$ ), wind direction ( $Z_i^{O-B_D}$ ), u wind ( $Z_i^{O-B_u}$ ) and v wind ( $Z_i^{O-B_v}$ ) are calculated in order, and the u wind and v wind with Z-scores greater than 3.0 are eliminated.

The calculation method for Z-scores (Zou & Zeng, 2006) is as follows; given  $n$  observation samples ( $x_i, i = 1, 2, \dots, n$ ), the median value of the samples is marked as  $M$ . The median value of the absolute sample values ( $|x_i|, i = 1, 2, \dots, n$ ) is marked as  $M_{ad}$ , where  $|\cdot|$  represents taking an absolute value. The biweight of each observation data can be defined as in Equation (1).

$$w_i = \frac{x_i - M}{c \times M_{ad}}, \quad (1)$$

where  $c$  denotes a parameter representing a ‘censor’ value such that all data beyond a certain distance from the centre (controlled by the parameter  $c$ ) are given zero weight. Referring to Zou and Zeng (2006),  $c$  is set to 7.5 in this research. For Gaussian case,  $c = 7.5$  censors values more than five standard deviations from the mean. Moreover, it is specified that when  $|w_i| > 1$ ,  $w_i$  is set to 1. When using

Equation (1) to calculate the biweight, the mean of the biweight is defined as in Equation (2).

$$\bar{x}_{bi} = M + \frac{\sum_{i=1}^n (x_i - M)(1 - w_i^2)^2}{\sum_{i=1}^n (1 - w_i^2)^2}. \quad (2)$$

The biweight standard deviation can be defined as in Equation (3).

$$S = \frac{\left[ n \sum_{i=1}^n (x_i - M)^2 (1 - w_i^2)^4 \right]^{0.5}}{\left| \sum_{i=1}^n (1 - w_i^2)(1 - 5w_i^2) \right|}. \quad (3)$$

From Equations (1)–(3), it can be seen that when calculating the biweight mean and standard deviation, samples that are close to the centre (median) are given higher weights compared with samples far away from the centre. Therefore, the biweight mean and standard deviation are basically not affected by outliers, and they are more stable than those from traditional equal-weight methods. The Z-scores of samples can be calculated by using the biweight mean and standard deviation as the standard for quality control.

$$Z_i = \frac{x_i - \bar{x}_{bi}}{S}. \quad (4)$$

## 2.3 | Results of comprehensive quality control

Figure 5 shows the PDFs of the O–B values of the unsparsified AMV (u wind and v wind) observations

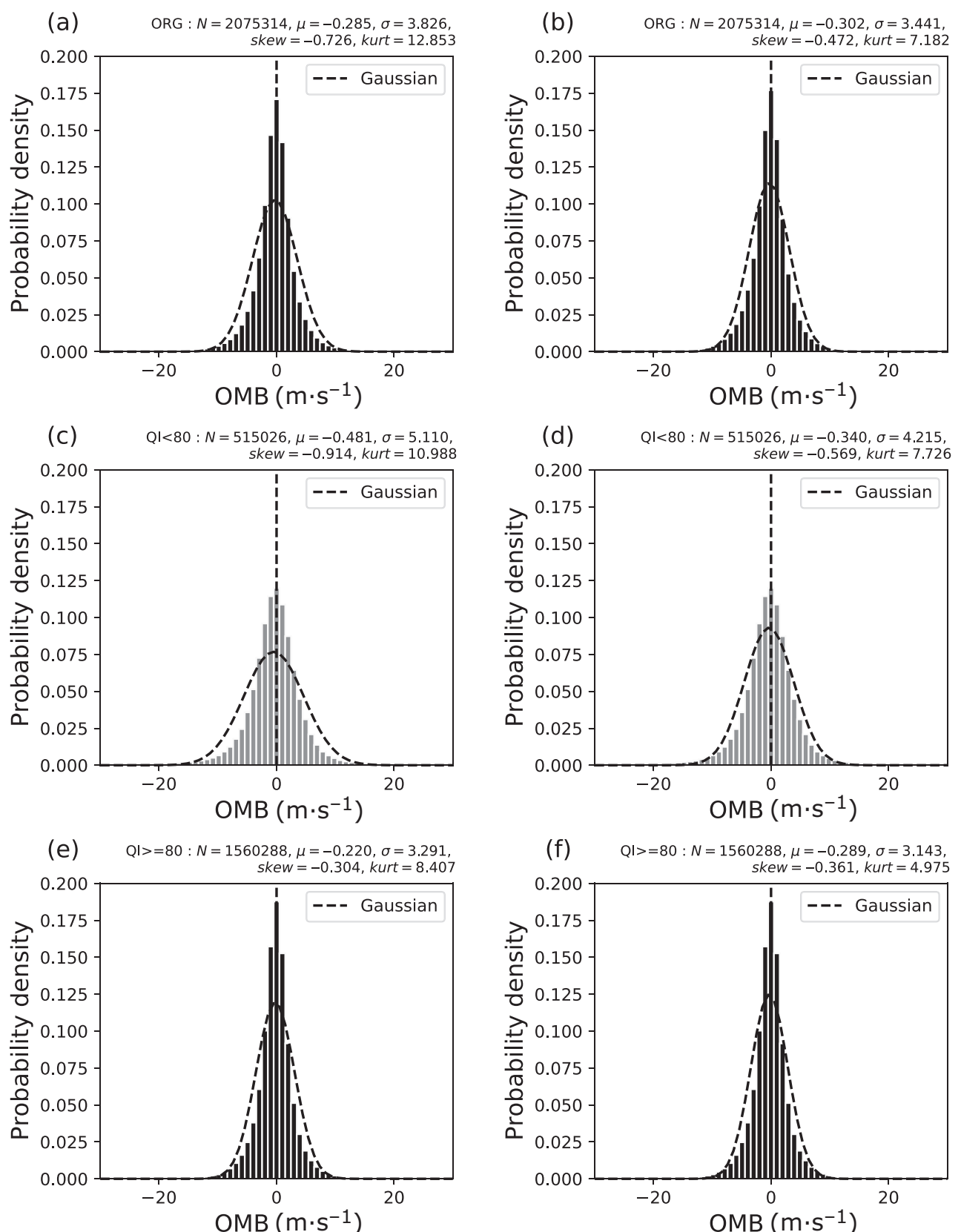
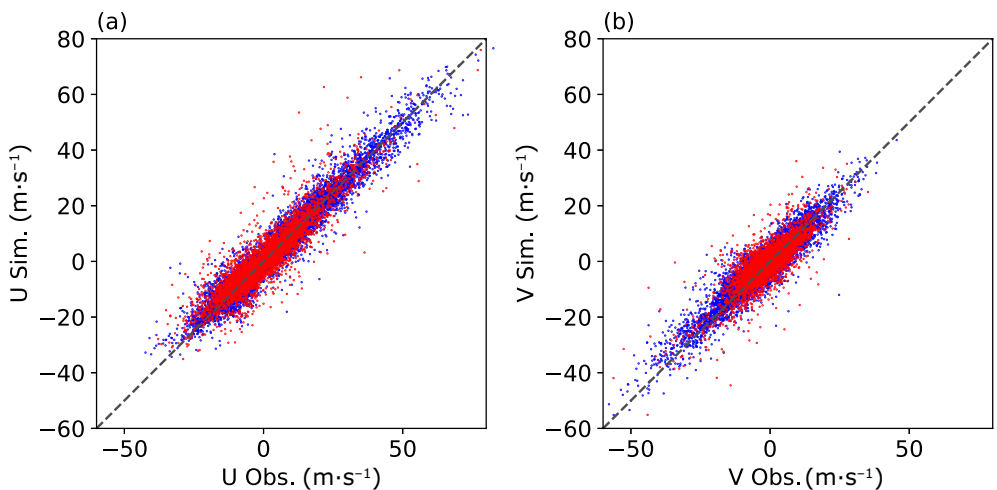


**FIGURE 5** The probability density functions (PDFs) of the observation-minus-background ( $O - B$ ) values of the (a,c,e)  $u$  wind ( $O - B_u$ ) and (b,d,f)  $v$  wind ( $O - B_v$ ) from (a,b) the observations without quality control, (c,d) the observations rejected after the quality control by the quality indicator (QI) method, and (e,f) the remaining observations after quality control by the quality indicator (QI). The black dashed lines represent the Gaussian distribution simulated with the mean and standard deviation of the samples. The samples include the observation data without sparsity processing and span from 0300 UTC to 0900 UTC on 12 August 2022.

**FIGURE 6**

Observation-background scatter plots of the (a) u wind and (b) v wind. Red and blue dots represent the samples with quality indicator (QI) < 80 and QI ≥ 80, respectively. Obs and Sim represent the observations and background. The data used here are the same as those in Figure 5. [Colour figure can be viewed at [wileyonlinelibrary.com](http://wileyonlinelibrary.com)]



with the six-hour window from 0300 UTC to 0900 UTC on 12 August 2022. The O–B values of the observed u wind ( $O - B_u$ ) and v wind ( $O - B_v$ ) show obvious leptokurtic and platykurtic distributions (Figure 5a,b). The mean value and skewness of the  $O - B_u$  are  $-0.29$  and  $-0.73 \text{ m}\cdot\text{s}^{-1}$ , respectively, and those of the  $O - B_v$  are  $-0.30$  and  $-0.47 \text{ m}\cdot\text{s}^{-1}$ , respectively. The kurtosis values of the  $O - B_u$  and  $O - B_v$  are  $12.85$  and  $7.18$ , respectively. The leptokurtic and platykurtic distributions of the  $O - B_u$  and  $O - B_v$  are obviously different from the unbiased Gaussian distribution. After the quality control, the rejected AMV data with a QI value less than  $80$  have similar PDF distributions of the  $O - B_u$  and  $O - B_v$  to those of the original data (Figure 5c,d), but with larger skewness and kurtosis values. Specifically, the mean value and skewness of the  $O - B_u$  are  $-0.48$  and  $-0.91 \text{ m}\cdot\text{s}^{-1}$ , respectively, the mean value and skewness of the  $O - B_v$  are  $-0.34$  and  $-0.57 \text{ m}\cdot\text{s}^{-1}$ , respectively, and the kurtosis values of the  $O - B_u$  and  $O - B_v$  are  $11.00$  and  $7.73$ , respectively. After excluding the AMV data with a QI value less than  $80$ , the PDF distributions of the  $O - B_u$  and  $O - B_v$  of the remaining data are closer to the Gaussian distribution, but they still show obvious leptokurtic and platykurtic distributions. After removing the outliers by QI (Figure 5e,f), the mean value and skewness of the  $O - B_u$  are  $-0.22$  and  $-0.30 \text{ m}\cdot\text{s}^{-1}$ , respectively, the mean value and skewness of the  $O - B_v$  are  $-0.29$  and  $-0.36 \text{ m}\cdot\text{s}^{-1}$ , respectively, and the kurtosis values of the  $O - B_u$  and  $O - B_v$  are  $8.41$  and  $4.98$ , respectively. The above results suggest that the QI method of quality control, measured by whether the PDF distributions of the  $O - B_u$  and  $O - B_v$  follow a Gaussian distribution, can exclude some data with large O–B values and remarkably reduce the skewness and kurtosis of the  $O - B_u$  and  $O - B_v$ . However, this method cannot completely reject the observations with large O–B values (Figure 6). After the quality control, the PDFs of the O–B values still show an obvious leptokurtic and platykurtic

distribution. Thus, the AMVs subjected to quality control by this method do not fully satisfy the requirements of variational assimilation.

Figure 7 depicts the PDF distributions of the  $O - B_u$  of the AMV data before and after the biweight background check in the bivector space and those of the eliminated data from the background check. Figure 7b shows that according to the rejection criterion that the Z-scores of the O–B values of wind speed ( $Z_i^{O-B_w}$ ) are greater than  $3.0$ , the  $O - B_u$  of the eliminated AMV data shows a double peak distribution. The two peaks are around  $\pm 10 \text{ m}\cdot\text{s}^{-1}$ , and the left peak has a higher PDF value. This result suggests that using  $Z_i^{O-B_w} > 3.0$  as a criterion can effectively remove samples that cause skewness in the PDF distribution of the  $O - B_u$ . Furthermore, the  $O - B_u$  values of the eliminated data are concentrated in the segment of larger  $|O - B_u|$  values ( $> 5 \text{ m}\cdot\text{s}^{-1}$ ), presenting an obvious long- and fat-tailed distribution. This result means that using  $Z_i^{O-B_w} > 3.0$  as a judgment condition can effectively exclude the observations that cause the leptokurtic and platykurtic distribution of the  $O - B_u$ . When the rejection criterion is that the Z-scores of the O–B values of wind direction ( $Z_i^{O-B_D}$ ) are greater than  $3.0$  (Figure 7c), the PDF of the  $O - B_u$  of the eliminated data approximates a flat Gaussian distribution, and the  $O - B_u$  values are concentrated in the range of  $\pm 20 \text{ m}\cdot\text{s}^{-1}$ . This result indicates that using  $Z_i^{O-B_D} > 3.0$  as a judgment condition can effectively eliminate some of the observation data that cause the leptokurtic distribution of  $O - B_u$ .

Figure 7d presents the PDF distribution of the  $O - B_u$  values of the eliminated data when the rejection criterion is the Z-scores of the O–B values of u wind ( $Z_i^{O-B_u}$ ) greater than  $3.0$ . It can be found that the  $O - B_u$  values of the eliminated data are mostly larger than  $+8 \text{ m}\cdot\text{s}^{-1}$  or smaller than  $-8 \text{ m}\cdot\text{s}^{-1}$ , indicating that this rejection criterion can effectively remove the observation data that cause the platykurtic distribution of the  $O - B_u$ . If

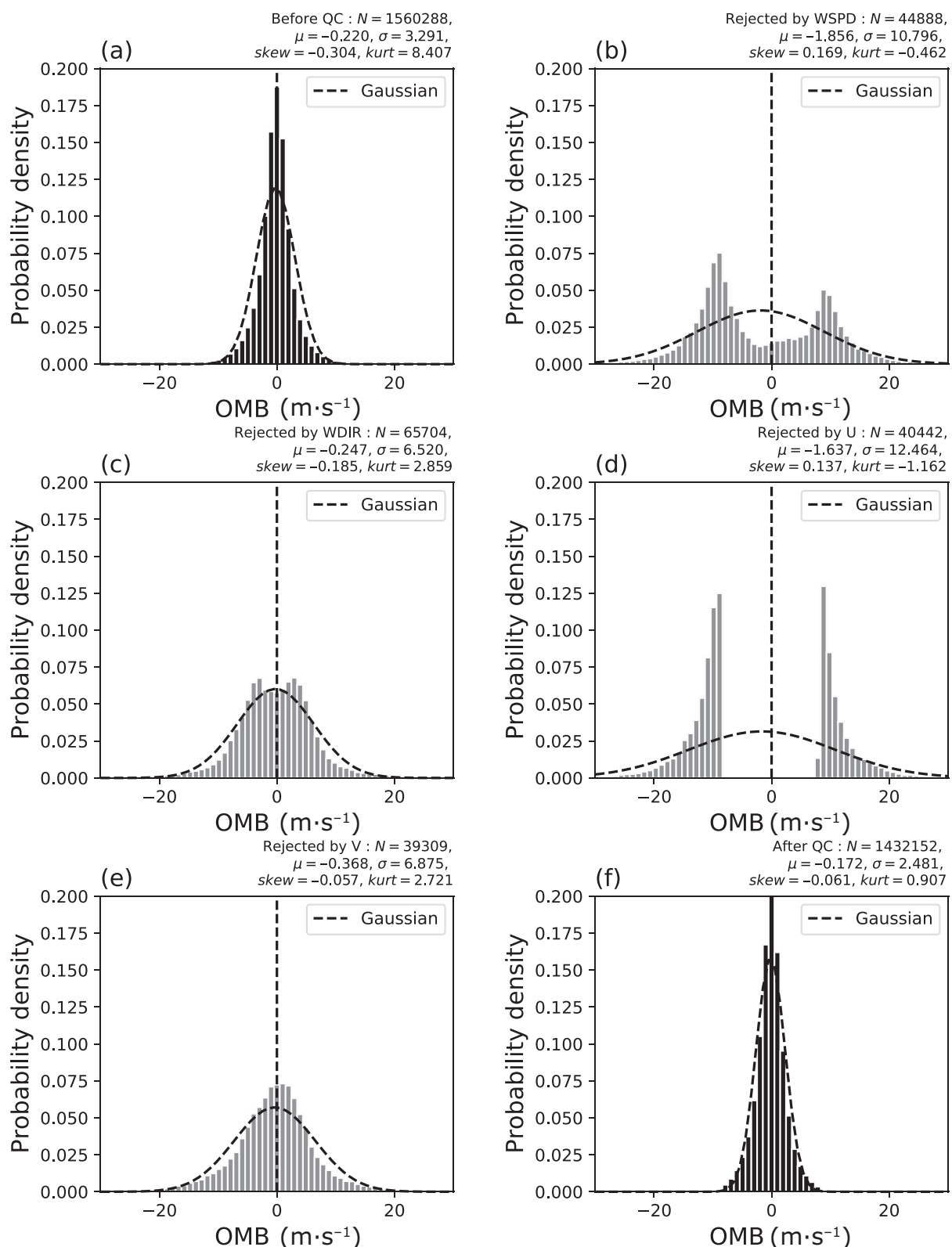


**FIGURE 7** (a) The probability density function (PDF) distribution of the observation-minus-background ( $O - B_u$ ) values of the observation data after the blacklist processing and the quality indicator (QI) quality control but before the biweight background check in bivector space; (b,c,d,e) the PDF distributions of the  $O - B_u$  values under different rejection criteria: the Z-scores of the  $O - B$  values of (b) wind speed; (c) wind direction; (d) u wind; and (e) v wind greater than 3.0, respectively, and (f) the PDF distribution of the  $O - B_u$  values after the biweight background check. The black and grey bars represent the PDFs of the  $O - B$  values, and the dashed lines are the Gaussian distributions of the mean and standard deviation. The samples include the observation data without sparsity processing and span from 0300 UTC to 0900 UTC on 12 August 2022.

the rejection criterion is the  $Z$ -scores of the  $O - B$  values of  $v$  wind ( $Z_i^{O-B_v}$ ) greater than 3.0 (Figure 7e), the PDF distribution of the  $O - B_u$  values of the eliminated data approximates a Gaussian distribution, which means that the criterion of  $Z_i^{O-B_v} > 3.0$  can effectively remove the observation data that cause the leptokurtic distribution of the  $O - B_u$ . From Figure 7f, it can be found that after the QI quality control, the blacklist processing and the biweight background check in the bivector space, the PDF distribution of the  $O - B_u$  values is closer to an unbiased Gaussian distribution compared with that before the background check (Figure 7a). The skewness decreases from  $-0.30$  to  $0.06$ , and the kurtosis decreases from  $8.41$  to  $0.91$ . The average of the  $O - B_u$  values changes from  $-0.22$  to  $-0.17 \text{ m}\cdot\text{s}^{-1}$ , and the standard deviation of the  $O - B_u$  values decreases from  $3.29$  to  $2.48 \text{ m}\cdot\text{s}^{-1}$ . These results indicate that the biweight background check in bivector space can effectively reject the observation data that cause the leptokurtic and platykurtic distribution of  $O - B_u$ , making the  $O - B_u$  values closer to a Gaussian distribution after quality control.

Figure 8 shows the PDF distributions of the  $O - B_v$  values of the observations before and after the biweight background check in bivector space and those of the eliminated data from the background check. It can be found from Figure 8b that for the rejection criterion of  $Z_i^{O-B_v} > 3.0$ , the  $O - B_v$  values of the eliminated observation data present a skewed quasi-Gaussian distribution, with a mean value of  $2.01 \text{ m}\cdot\text{s}^{-1}$  and a standard deviation of  $8.3 \text{ m}\cdot\text{s}^{-1}$  (remarkably larger than the standard deviation of  $O - B_v$  values before the background field check), indicating that this criterion can effectively remove the samples that cause the skewed distribution and the long- and fat-tailed distribution of  $O - B_v$ .

When the rejection criterion is  $Z_i^{O-B_v} > 3.0$  (Figure 8c), the PDF distribution of the  $O - B_v$  values of the eliminated data is similar to that of the  $O - B_u$  values, that is, the  $O - B_v$  values are concentrated in the range of  $\pm 20 \text{ m}\cdot\text{s}^{-1}$ , showing a double peak distribution (peaks around  $\pm 5 \text{ m}\cdot\text{s}^{-1}$ ). This result indicates that the rejection criterion of  $Z_i^{O-B_v} > 3.0$  can effectively remove some of the observation data that cause the leptokurtic distribution of  $O - B_v$ . Taking  $Z_i^{O-B_v} > 3.0$  as the rejection criterion (Figure 8d), we find that the PDF distribution of the  $O - B_v$  values is close to the Gaussian distribution, but with a leptokurtic characteristic, indicating this criterion can effectively eliminate the observation data that cause the leptokurtic distribution of  $O - B_v$ . Figure 8e displays the PDF distribution of the  $O - B_v$  values of the eliminated observation data under the rejection criterion of  $Z_i^{O-B_v} > 3.0$ . The  $O - B_v$  values are mostly smaller than  $-8 \text{ m}\cdot\text{s}^{-1}$  and larger than  $8 \text{ m}\cdot\text{s}^{-1}$ . This means that the rejection criterion of  $Z_i^{O-B_v} > 3.0$  can effectively reject the

observations that cause a long- and fat-tailed distribution. Figure 8f presents the PDF distribution of the  $O - B_v$  values after blacklist processing, the QI quality control and the biweight background check in bivector space. It can be found that after the biweight background check, the PDF distribution of the  $O - B_v$  values is closer to an unbiased Gaussian distribution than compared with that before the background check (Figure 8a). Specifically, the skewness changes from  $-0.361$  to  $0.114$ , and the kurtosis decreases from  $4.975$  to  $0.918$ . The average of the  $O - B_v$  values changes from  $-0.29$  to  $-0.22 \text{ m}\cdot\text{s}^{-1}$ , and their standard deviation decreases from  $3.14$  to  $2.45 \text{ m}\cdot\text{s}^{-1}$ . It can be concluded that the biweight background check in bivector space can effectively eliminate the observations that cause the leptokurtic and platykurtic distribution of the  $O - B_v$  values, making their distribution closer to a Gaussian distribution.

Comparing the number of AMV observations from 0300 UTC to 0900 UTC on 12 August 2022 before and after the CQC, we find that they are 2,075,314 before the CQC but 1,432,152 after CQC (1,547,664 after OQC), and thus about 31% of the AMV observations are excluded through the CQC (25% through the OQC).

### 3 | IMPACT OF THE COMPREHENSIVE QUALITY CONTROL ON THE ANALYSIS AND PREDICTION OF THE CMA-GFS

#### 3.1 | Introduction to the assimilation system and experiment design

In order to evaluate the impact of different AMV quality control schemes on the analysis and forecast fields, the CMA-GFS V3.4 assimilation and prediction system is used in this study to carry out NWP experiments. CMA-GFS V3.4 adopts the Global/Regional Assimilation and Prediction System (GRAPES), with a horizontal resolution of  $0.25^\circ \times 0.25^\circ$  and 87 vertical layers. Additionally, it adopts a 4DVAR assimilation system (Zhang et al., 2019), with an assimilation time window of six hours and the observations divided into 30-minute timeslots. The horizontal resolution of the outer loop of the 4DVAR system is the same as that of the CMA-GFS V3.4 ( $0.25^\circ \times 0.25^\circ$ ), while the horizontal resolution of the inner loop is  $1.0^\circ \times 1.0^\circ$ .

Three sets of numerical experiments were designed (Table 3), which assimilate different observation data. Experiment AMV\_OQC shares the same quality control scheme and simulated observations as the CMA-GFS V3.4 operational suite (Table 4). Experiments AMV\_DENY and AMV\_CQC have the same configuration as experiment

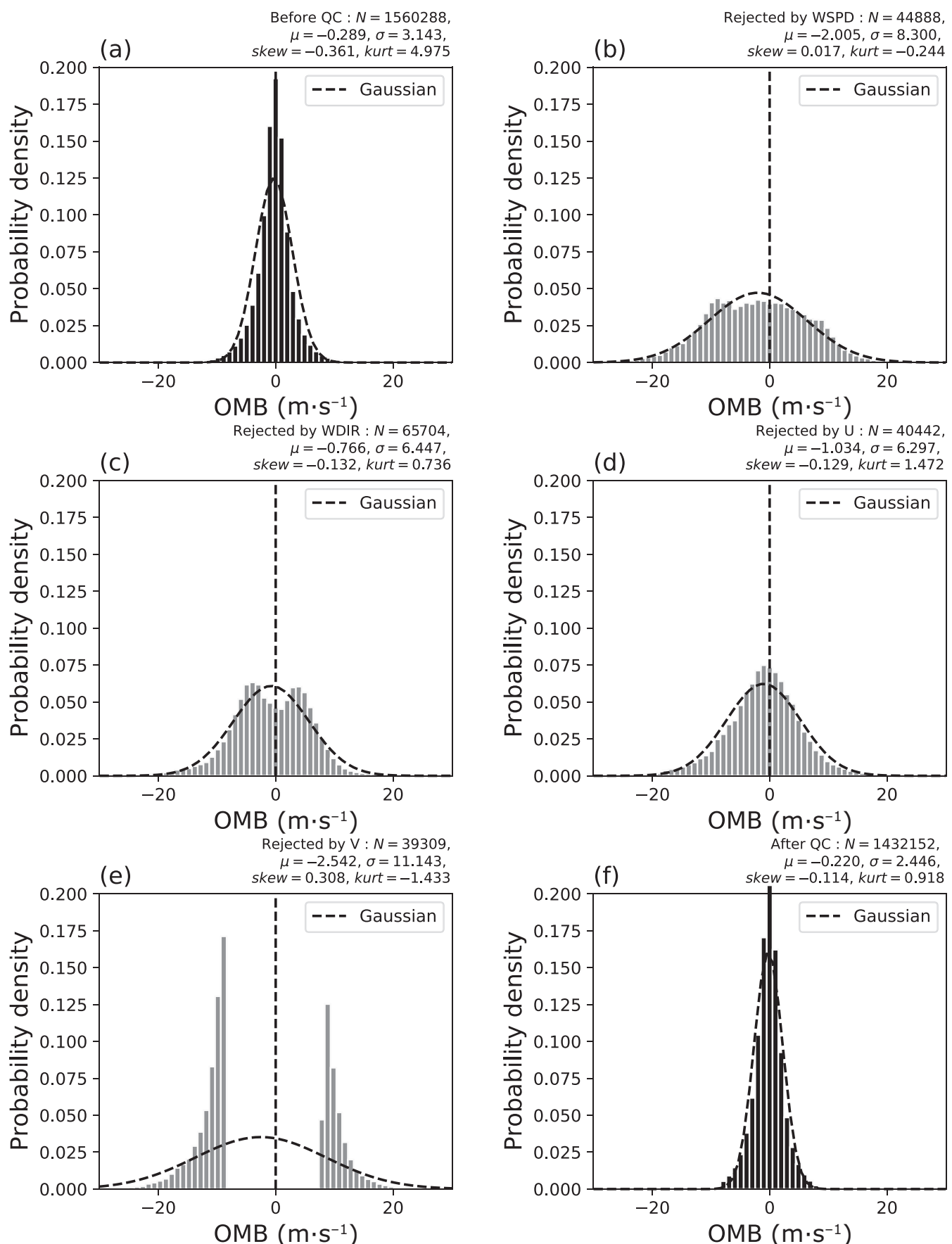


FIGURE 8 Same as Figure 7, but for the  $O - B_v$  values.  $O - B$ , observation-minus-background.

TABLE 3 Numerical experiment setup.

Experiment name	Assimilated data
AMV_OQC	Same observations as those operationally assimilated in the CMA-GFS V3.4 (Table 4)
AMV_DENY	Same data as those in experiment AMV_OQC but without AMV assimilation
AMV_CQC	Same data as those in experiment AMV_OQC but with the assimilation of the AMV data after the CQC

Abbreviations: AMV, atmospheric motion vector; CQC, comprehensive quality control; OQC, original quality control.

AMV\_OQC, but experiment AMV\_DENY does not assimilate the AMV data, while experiment AMV\_CQC assimilates the AMV data after the CQC. The period selected for the experiments is from 0300 UTC on 10 August to 2100 UTC on 15 September 2022, a total of 35 days.

### 3.2 | Impacts on analysis fields

In the analysis field of the CMA-GFS 4DVAR operational system (i.e., experiment AMV\_OQC), compared with the ERA5 reanalysis, there are obvious positive deviations of the 200 hPa velocity potential function over the western tropical Pacific, eastern Indian Ocean and southern North America and obvious negative deviations over the eastern Pacific (Figure 2b), which do not exist in the results of experiment AMV\_CQC (Figure 2f). Moreover, the deviation distributions of the 200-hPa velocity potential function are basically the same in the analysis field of experiments AMV\_DENY (Figure 2e) and AMV\_CQC (Figure 2g), indicating that assimilating the AMV data after the CQC does not change the deviation distribution.

In order to evaluate and analyze the impacts of the AMV quality control schemes on the analysis fields of the CMA-GFS, the RMSE of the analysis field of variable  $x$  at each analysis time is calculated by using the ERA5 data as the reference field.

$$e_x = \frac{\sqrt{\sum_{i=1}^M \sum_{j=1}^N \left[ (x_{i,j}^c - x_{i,j}^e) \phi_j \right]^2}}{MN}, \quad (5)$$

where  $x_{i,j}^c$  and  $x_{i,j}^e$  denote the variable  $x$  (u wind, v wind, geopotential height  $h$ , or temperature  $t$ ) from the CMA-GFS analysis field and ERA5 reanalysis data,

respectively.  $i$  and  $j$  indicate the grid indexes in longitudinal and latitudinal directions in a given region, respectively.  $M$  and  $N$  are the numbers of grid points in longitudinal and latitudinal directions, respectively.  $\phi_j$  represents the latitude of grid point  $j$ . The RMSEs of each variable in the Northern Hemisphere ( $20^\circ$  N– $90^\circ$  N), Southern Hemisphere ( $20^\circ$  S– $90^\circ$  S) and tropical regions ( $20^\circ$  S– $20^\circ$  N) are evaluated separately in this study.

Figure 9 shows the mean RMSE profiles of u wind and geopotential height in the analysis fields of three experiments from 0300 UTC on 15 August to 2100 UTC on 15 September 2022. From Figure 9a–c, it can be found that among the three experiments, there are large differences in the RMSEs of the tropospheric u wind over the Northern Hemisphere, Southern Hemisphere and tropical regions. The RMSEs of u wind are the largest in experiment AMV\_OQC, especially over the tropical regions where the RMSEs are obviously larger than those in experiment AMV\_DENY. The RMSEs of u wind are the smallest in experiment AMV\_CQC. The characteristics of the mean RMSEs of v wind are the same as those of u wind (figure omitted). Similar characteristics can be found in the mean RMSEs of the geopotential height analysis field in the three experiments, that is, the RMSEs of the geopotential height are the smallest in experiment AMV\_CQC, followed by experiment AMV\_DENY, and the largest for experiment AMV\_OQC (Figure 9d–f). The above results indicate that compared with the experiment without AMV assimilation (AMV\_DENY), assimilating the AMV data after the OQC (AMV\_OQC) substantially increases the RMSEs of the variables (u wind, v wind, geopotential height and temperature) in the tropospheric analysis field of the CMA-GFS, while the assimilation of the AMV data after the CQC can considerably decrease the RMSEs. This result also reveals that the assimilation effect of the AMVs is susceptible to data quality control.

Furthermore, we analyze the assimilation effect of the AMV data subjected to different quality control schemes on the errors of analysis fields at different heights. To this end, we calculate the change ratios of the RMSEs of the analysis fields in experiments AMV\_OQC and AMV\_CQC relative to those in experiment AMV\_DENY using Equation (6).

$$r_t = \frac{e_x^{\text{AMV}} - e_x^{\text{DENY}}}{e_x^{\text{DENY}}} \times 100\%, \quad (6)$$

where  $e_x^{\text{AMV}}$  represents the RMSE of variable  $x$  in experiment AMV\_OQC or experiment AMV\_CQC, and  $e_x^{\text{DENY}}$  denotes the RMSE of variable  $x$  in experiment AMV\_DENY. The mean change ratio of the RMSEs

TABLE 4 Observation variables assimilated in experiment AMV\_OQC.

Observation types	Instruments	Platforms	Assimilated observation element
Conventional observation	TEMP		Wind, temperature, relative humidity
	SYNOP		Air pressure
	SHIP		Air pressure
	BUOY		Wind
Satellite-based observation	AIREP		Wind, temperature
	AMSUA	NOAA-15/18/19, Metop-A/B	Radiance
	AMSUB	NOAA-18/19, Metop-A/B	Radiance
	MWTS-2	FY-3D/E	Radiance
	ATMS	Soumi-NPP	Radiance
	MWHS-2	FY-3C/D/E	Radiance
	MWR	FY-3D	Radiance
	HIRAS	FY-3D	Radiance
	IASI	Metop-A/B	Radiance
	AIRS	AQUA (EOS-2)	Radiance
	GIIRS	FY-4A	Radiance
	AGRI	FY-4A	Radiance
	S-VISSR	FY-2H	Radiance
	GNSS RO	COSMIC, COSMIC-2, Metop-A/B/C GRAS, GRACE-A, TerraSAR-X, FY-3D GNOS	Refractivity
AMVs	GPS-PW		Atmospheric column water vapour content
		Himarwii-8 GOES-16/17 METEOSAT-8/11	Wind (u and v component)
		FY-2G/H INSAT-3/3R NOAA-15/18/19/20	
		TERRA AQUA Metop-A	

Abbreviations: AMV, atmospheric motion vector; OQC, original quality control.

at multiple analysis times can be calculated by Equation (7).

$$\bar{r} = \frac{\sum_{t=1}^P r_t}{P}, \quad (7)$$

where  $P$  indicates the number of analysis times. The standard deviation of the change ratios of the RMSEs can be obtained by Equation (8).

$$\sigma = \sqrt{\frac{\sum_{t=1}^P (r_t - \bar{r})^2}{P-1}} \quad (8)$$

Figure 10 illustrates the mean change ratio profiles of the RMSEs of u wind and geopotential height in experiments AMV\_OQC and AMV\_CQC relative to those in experiment AMV\_DENY. From Figure 10a–c, it can be seen that after assimilating the AMV data subjected to the OQC, the RMSEs of u wind and geopotential

height increase remarkably in the troposphere (below 150 hPa). The RMSEs of u wind increase by about 25% in 850–200 hPa over the tropical regions, with the largest change ratio reaching 32% at around 400 hPa (Figure 10a). The increasing ratios of the RMSEs of u wind are about 10% at 400 hPa in the Southern Hemisphere, and those in the Northern Hemisphere are about 4% on average and mainly concentrated at 850–200 hPa. From Figure 10c, it can be found that the RMSEs of the geopotential height analysis field in experiment AMV\_OQC increase noticeably at 850–400 hPa compared with those in experiment AMV\_DENY. The change ratios of the RMSEs of geopotential height in the Southern Hemisphere and tropical regions reach their peak of 6% at around 600 hPa. However, the change ratios of the RMSEs of the geopotential height analysis field are the smallest in the Northern Hemisphere, which may be due to the sufficient number of sounding data and aircraft data serving as anchors in this area. The above results suggest that assimilating the AMVs subjected

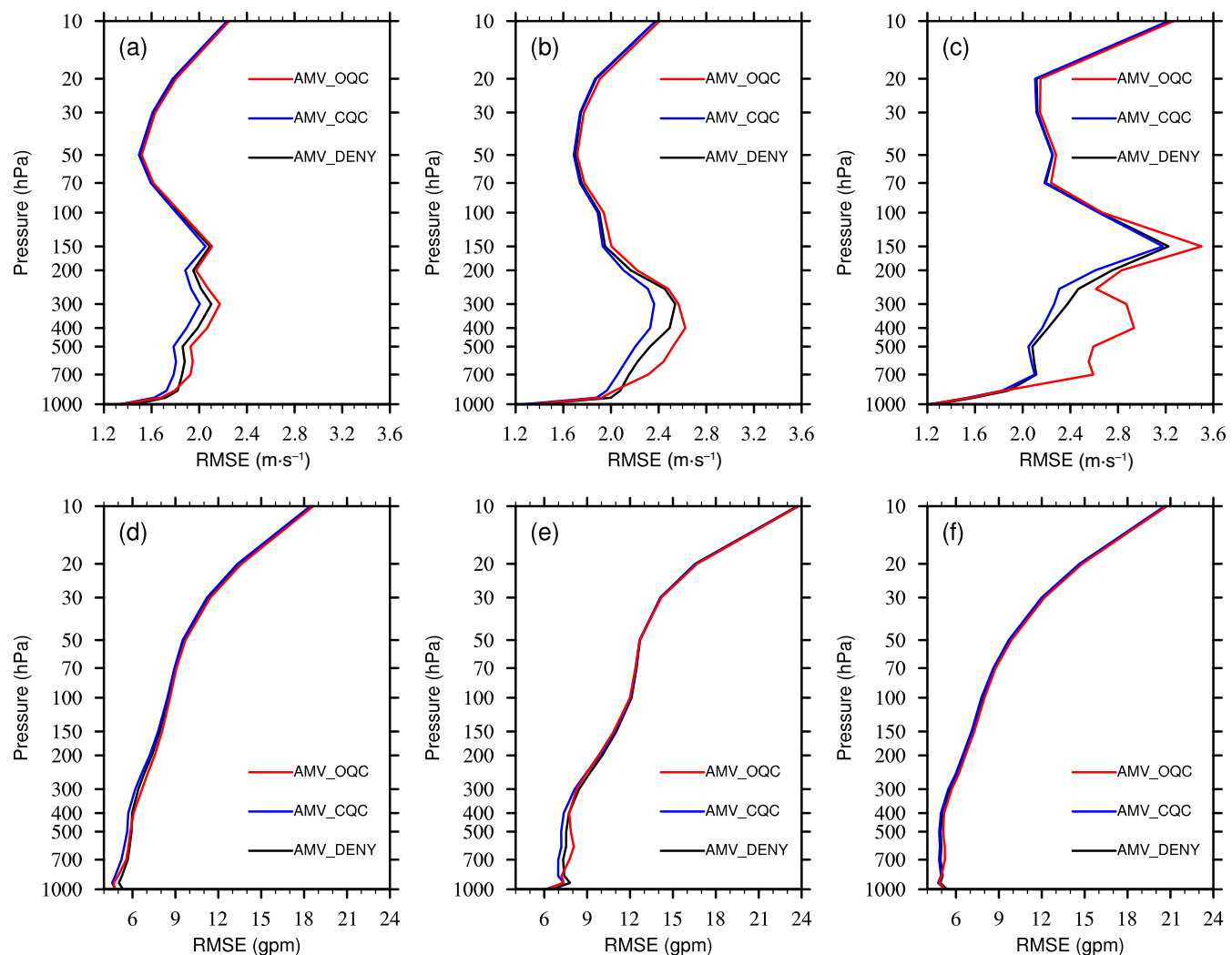


**FIGURE 9** Average root-mean-squared error (RMSEs) profiles of the (a–c) u wind and (d–f) geopotential height in the (a,d) Northern Hemisphere, (b,e) Southern Hemisphere and (c,f) tropical regions from experiments AMV\_DENY (black lines), AMV\_OQC (red lines) and AMV\_CQC (blue lines). AMV, atmospheric motion vector; CQC, comprehensive quality control; OQC, original quality control. [Colour figure can be viewed at [wileyonlinelibrary.com](http://wileyonlinelibrary.com)]

to the OQC greatly increases the RMSEs of the u wind and geopotential height analysis fields, negatively contributing to the CMA-GFS analysis fields.

On the contrary, the RMSEs of the u wind and geopotential height analysis fields both decrease in experiment AMV\_CQC compared with those in experiment AMV\_DENY (Figure 10b,d). The change ratios of the RMSEs of u wind at heights below 150 hPa are about  $-4\%$ ,  $-6\%$ , and  $-3\%$  on average in the Northern Hemisphere, Southern Hemisphere and tropical regions, and the change ratios of the RMSEs of geopotential height are about  $-6\%$ ,  $-5\%$  and  $-3\%$ . The decreasing ratios of the RMSEs of v wind are similar to those of u wind, and the decreasing ratios of the RMSEs of temperature are comparable to those of geopotential height (figures omitted).

### 3.3 | Impacts on forecast fields

The RMSE and anomaly correlation coefficient (ACC) are generally used to evaluate the medium-range forecast skill of global NWP models. Figure 11 presents the difference in the ACCs of u wind and geopotential height between experiments AMV\_OQC and AMV\_DENY (the ACC has been multiplied by 100). Compared with experiment AMV\_DENY, the ACCs of u wind in experiment AMV\_OQC decrease dramatically for almost all forecast leading times and at all heights in the Northern Hemisphere (Figure 11a), while those also decrease at leading times of 0–144 hours in the troposphere of the Southern Hemisphere (Figure 11c) and decrease the most in the troposphere of tropical regions at leading times of 0–240 hours (Figure 11e). Using the ACC as an indicator of

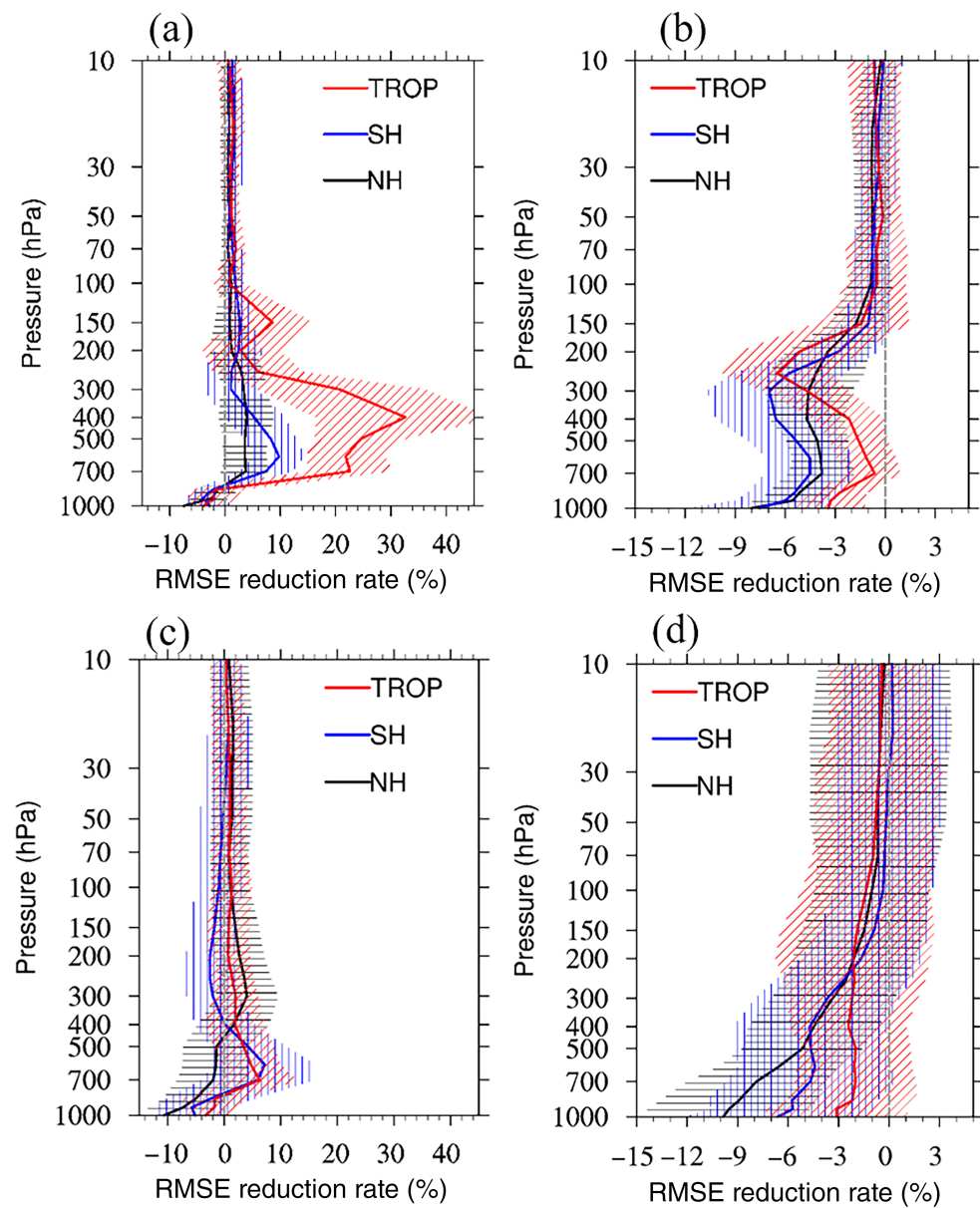


**FIGURE 10** Change ratios of the root-mean-squared error (RMSEs) of (a,b) u wind and (c,d) geopotential height from experiments (a,c) AMV\_OQC and (b,d) AMV\_CQC relative to those in experiment AMV\_DENY. The black, blue and red lines denote the values in the Northern Hemisphere, tropical regions and the Southern Hemisphere, respectively. The black, blue and red grids present the uncertain ranges ( $r \pm \sigma$ ) of the RMSE change ratios in the Northern Hemisphere, Southern Hemisphere and tropical regions, respectively. AMV, atmospheric motion vector; CQC, comprehensive quality control; OQC, original quality control. [Colour figure can be viewed at [wileyonlinelibrary.com](http://wileyonlinelibrary.com)]

forecast skill, we find that the forecast skill of experiment AMV\_OQC for the u-wind field in the troposphere of tropical regions decrease by more than 10%. The difference distributions in the ACCs of geopotential height between experiments AMV\_OQC and AMV\_DENY are similar to those of u wind (Figure 11b,d,f), but with noticeably smaller magnitude for the geopotential height. Additionally, the difference distributions in the ACCs of v wind are comparable to those of u wind (figure omitted). Compared with experiment AMV\_DENY, the forecast leading times and heights with the increasing RMSEs of all variables in experiment AMV\_OQC are almost the same as those with the decreasing ACCs, and vice versa. The above results reveal that assimilating the AMV data after the OQC substantially reduces the forecast skill of the CMA-GFS.

Moreover, we analyze the differences in the ACCs of u wind and geopotential height between experiments AMV\_CQC and AMV\_DENY (Figure 12). Compared with experiment AMV\_DENY, the ACCs of u wind in the Northern Hemisphere increase at nearly all forecast leading times and heights, except for leading times of 168–192 hours (Figure 12a), and the ACCs in the Southern Hemisphere increase at all forecast leading times and heights (Figure 12c). Over the tropics, except for 700–300 hPa and leading times of 0–72 hours, the ACCs of u wind increase at all forecast leading times and heights (Figure 12e). Using the ACC as an indicator of forecast skill, we find that experiment AMV\_CQC improves the forecast skill for u wind by more than 3% in the troposphere of the Southern Hemisphere. Between experiments

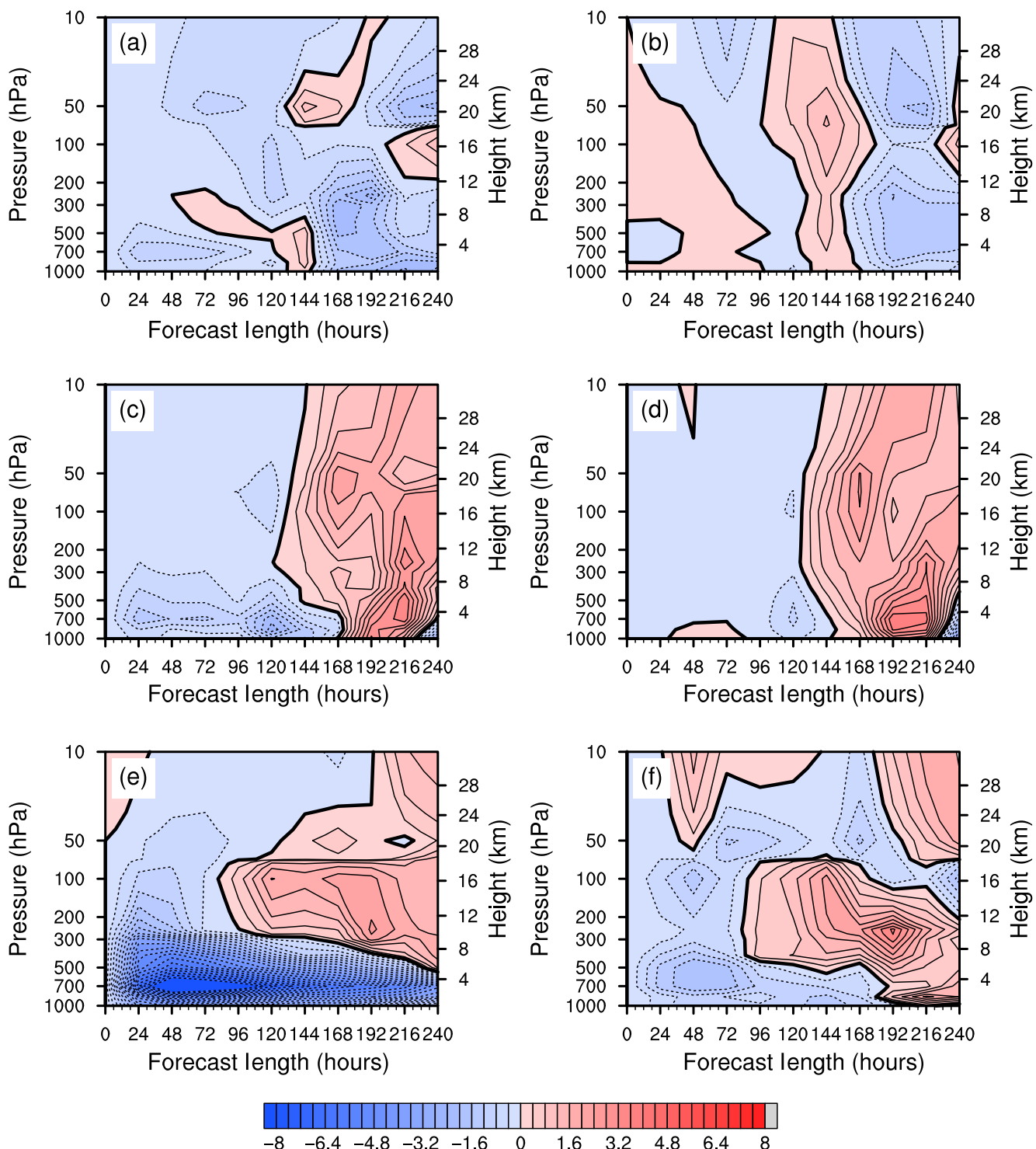


**FIGURE 11** Differences in the anomaly correlation coefficient (ACC) of (a,c,e) u wind and (b,d,f) geopotential height fields between experiments AMV\_OQC and AMV\_DENY in the (a,b) Northern Hemisphere, (c,d) Southern Hemisphere and (e,f) tropical regions. AMV, atmospheric motion vector; OQC, original quality control. [Colour figure can be viewed at [wileyonlinelibrary.com](http://wileyonlinelibrary.com)]

AMV\_CQC and AMV\_DENY, the difference distributions of the ACCs of geopotential height (Figure 12b,d,f) and v wind (figure omitted) are similar to those of u wind. The forecast leading times and heights with smaller RMSE val-

ues of all variables are almost the same as those with larger ACC values, and vice versa. Overall, assimilating the AMV data after the CQC can dramatically improve the forecast skill of the CMA-GFS.

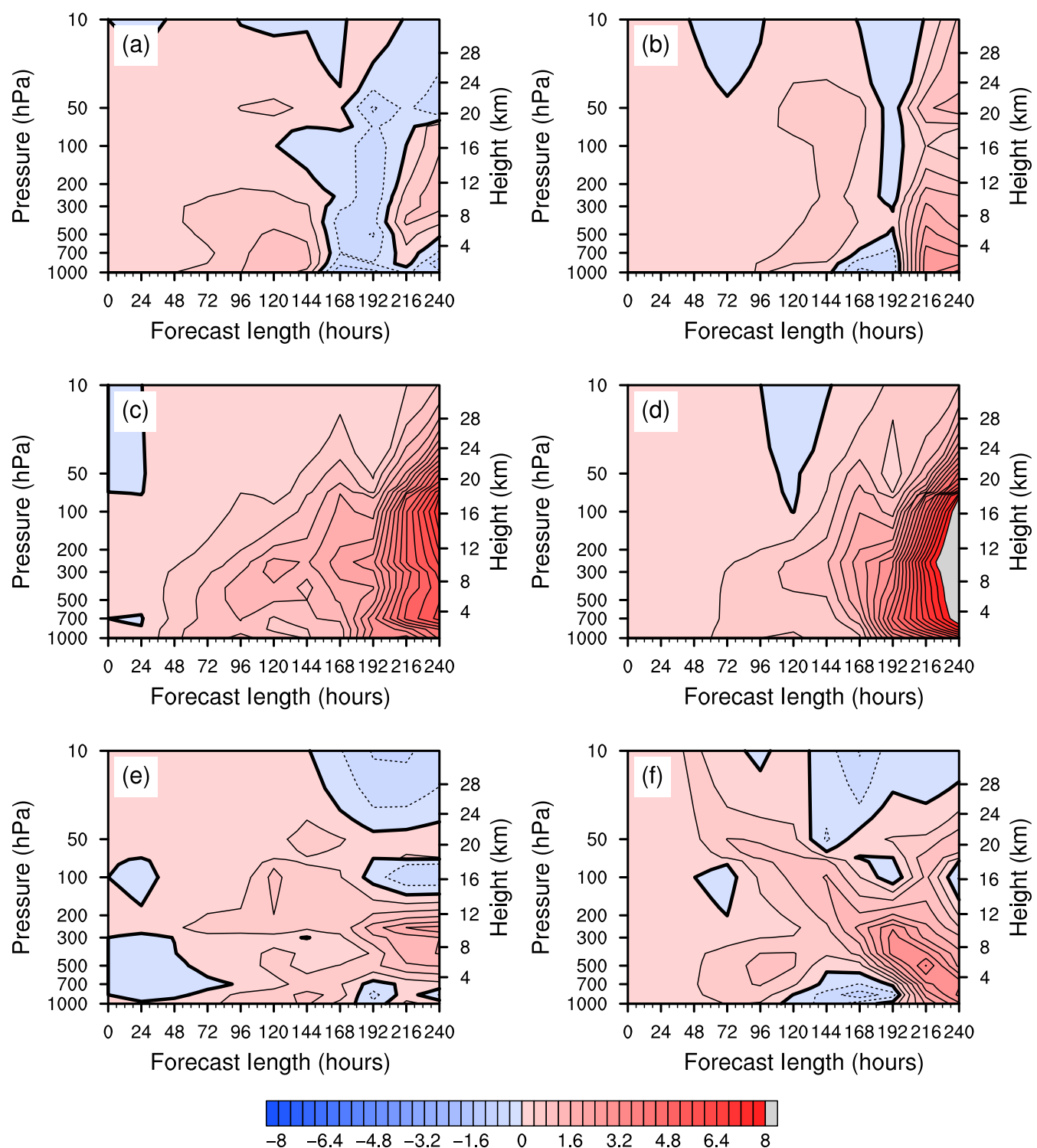


**FIGURE 12** Same as Figure 11, but for experiment AMV\_CQC. AMV, atmospheric motion vector; CQC, comprehensive quality control. [Colour figure can be viewed at [wileyonlinelibrary.com](http://wileyonlinelibrary.com)]

## 4 | CONCLUSIONS AND DISCUSSION

In this study, the deficiencies of the OQC method in the current CMA-GFS operational system are analyzed. In

addition, a CQC method for the AMVs is proposed, which adopts the QI, the blacklist and the background field check based on the biweight method in bivector space. The PDF characteristics of the O – B values of the observations after every step of the CQC method are thoroughly investigated

to demonstrate the rationality of the CQC method. On this basis, a 35-day cyclic assimilation and prediction experiment is carried out to compare and analyze the impacts of the OQC and CQC methods on the AMV assimilation. The main conclusions are as follows.

1. The biweight background check in bivector space adopted in the CQC scheme can effectively detect outliers in AMV observations under a weak wind speed condition, which addresses the problem of the leptokurtic and platykurtic distribution of the O–B values after the OQC. The PDF of the O–B values of the AMVs after the CQC is closer to an unbiased Gaussian distribution, and thus, the AMVs subjected to the CQC can meet the requirements of variational assimilation.
2. Compared with the situation without the assimilation of AMV data, assimilating the AMV observations after the OQC (only the steps of QI and blacklist), which is the current operational quality control scheme, shows obvious negative contributions to the accuracy of analysis and forecast fields in the global medium-range NWP. The RMSEs of the wind analysis fields in the troposphere increase by 4%–32% over the Northern Hemisphere, Southern Hemisphere and tropical regions. The forecast skill of the model for u-wind fields decreases over the Northern Hemisphere, Southern Hemisphere and tropical regions to varying extents, especially in the tropics where the forecast skill for u wind in the troposphere decreases by more than 10%.

The results of assimilating different AMV data indicate that using the CQC method proposed in this study to conduct quality control for the AMVs before assimilation has remarkable positive contributions to the accuracy of the analysis and forecast fields of the global medium-range NWP. The RMSEs of the wind fields in the troposphere decrease by 3%–6% over the Northern Hemisphere, Southern Hemisphere and tropical regions. The forecast skill for u wind increases over the Northern Hemisphere, Southern Hemisphere and tropic regions to different extents, among which the forecast skill increases by more than 3% in the troposphere over the Southern Hemisphere.

In conclusion, AMV assimilation is highly sensitive to data quality control. Different quality control methods have different influences on the accuracy of analysis and forecast fields in the global medium-range NWP. The CQC method can effectively improve the assimilation effectiveness of the AMVs, thereby enhancing the accuracy of analysis and forecast fields. The biweight background check method in bivector space proposed in this study also has an important reference and application potential for the quality control of other wind field observations.

## ACKNOWLEDGEMENTS

This research was supported by the National Natural Science Foundation of China (Grant Nos. 42375150 and 12241103).

## DATA AVAILABILITY STATEMENT

The real-time global forecast products of the GRAPES\_GFS at CMA are available from the authors upon request. The ERA-5 reanalysis can be downloaded from the ECMWF dataset archive at <https://cds.climate.copernicus.eu/cdsapp#!/dataset/reanalysisera5-pressure-levels?tab=form>.

## ENDNOTES

<sup>1</sup> <https://nwp-saf.eumetsat.int/site/monitoring-winds-quality-evaluation-amv-amv-use-in-nwp-ecmwf/>.

<sup>2</sup> <https://nwp-saf.eumetsat.int/site/monitoring-winds-quality-evaluation-amv-amv-use-in-nwp-ukmo/>.

## ORCID

Jincheng Wang  <https://orcid.org/0000-0003-2442-9760>

Jie Feng  <https://orcid.org/0000-0002-2480-2003>

## REFERENCES

- Baker, N.L., Pauley, P.M., Stone, R.E. & Langland, R.H. (2022) Interpretation of forecast sensitivity observation impact in data denial experiments. In: Park, S.K. & Xu, L. (Eds.) *Data assimilation for atmospheric, oceanic and hydrologic applications*, Vol. IV. Cham: Springer.
- Bormann, N., Lawrence, H. & Farnan, J. (2019) Global observing system experiments in the ECMWF assimilation system. ECMWF Technical Memoranda, 839.
- Bormann, N., Saarinen, S., Kelly, G. & Thepaut, J.-N. (2003) The spatial structure of observation errors in atmospheric motion vectors from geostationary satellite data. *Monthly Weather Review*, 131, 706–718.
- Bormann, N., Salonen, K., Peubey, C., McNally, T. & Lupu, C. (2012) An overview of the status of the operational assimilation of AMVs at ECMWF. *11th International Winds Workshop*, 20–24 February 2012, Auckland, New Zealand.
- Cordoba, M., Dance, S.L., Kelly, G.A., Nichols, N.K. & Waller, J.A. (2017) Diagnosing atmospheric motion vector observation errors for an operational high-resolution data assimilation system. *Quarterly Journal of the Royal Meteorological Society*, 143, 333–341. Available from: <https://doi.org/10.1002/qj.2925>
- Deb, S.K., Sankhala, D.K., Kumar, P. & Kishtawal, C.M. (2020) Retrieval and applications of atmospheric motion vectors derived from Indian geostationary satellites INSAT-3D/INSAT-3DR. *Theoretical and Applied Climatology*, 140, 751–765. Available from: <https://doi.org/10.1007/s00704-020-03120-8>
- Holmlund, K. (1998) The utilization of statistical properties of satellite-derived atmospheric motion vectors to derive quality indicators. *Weather and Forecasting*, 13, 1093–1104.
- Holmlund, K., Velden, C.S. & Rohn, M. (2001) Enhanced automated quality control applied to high-density satellite-derived winds. *Monthly Weather Review*, 129, 517–529.

- Lanzante, J.R. (1996) Resistant, robust and non-parametric techniques for the analysis of climate data: theory and examples, including applications to historical radiosonde station data. *International Journal of Climatology*, 16, 1197–1226.
- Lee, E., Todling, R., Karpowicz, B.M., Jin, J., Sewnath, A. & Park, S.K. (2022) Assessment of geo-Kompsat-2A atmospheric motion vector data and its assimilation impact in the GEOS atmospheric data assimilation system. *Remote Sensing*, 14(21), 5287. Available from: <https://doi.org/10.3390/rs14215287>
- Lorenc, A.C. (1986) Analysis methods for numerical weather prediction. *Quarterly Journal of the Royal Meteorological Society*, 112(474), 1177–1194. Available from: <https://doi.org/10.1002/qj.49711247414>
- Martin, A., Weissmann, M. & Cress, A. (2023) Impact of assimilating Aeolus observations in the global model ICON: a global statistical overview. *Quarterly Journal of the Royal Meteorological Society*, 149(756), 2962–2979. Available from: <https://doi.org/10.1002/qj.4541>
- Nie, S., Jia, X., Deng, W., Lu, Y., He, D., Zhao, L. et al. (2022) The influence of FY-4A high-frequency LST data on data assimilation in a climate model. *Remote Sensing*, 15(1), 59. Available from: <https://doi.org/10.3390/rs15010059>
- Nieman, S., Menzel, W.P., Hayden, C.M., Gray, D.D., Wanzong, S., Velden, C.S. et al. (1997) Fully automated cloud-drift winds in NESDIS operations. *Bulletin of the American Meteorological Society*, 78, 1121–1133.
- Rennie, M.P., Isaksen, L., Weiler, F., de Kloe, J., Kanitz, T. & Reitebuch, O. (2021) The impact of Aeolus wind retrievals on ECMWF global weather forecasts. *Quarterly Journal of the Royal Meteorological Society*, 147(740), 3555–3586. Available from: <https://doi.org/10.1002/qj.4142>
- Santek, D., Dworak, R., Nebuda, S., Wanzong, S., Borde, R., Genkova, I. et al. (2019) 2018 atmospheric motion vector (AMV) inter-comparison study. *Remote Sensing*, 11(19), 2240. Available from: <https://doi.org/10.3390/rs11192240>
- Stoffelen, A., Benedetti, A., Borde, R., Dabas, A., Flamant, P., Forsythe, M. et al. (2020) Wind profile satellite observation requirements and capabilities. *Bulletin of the American Meteorological Society*, 101, E2005–E2021. Available from: <https://doi.org/10.1175/BAMS-D-18-0202.1>
- Wang, M., Yao, S., Jiang, L., Zhang, T., Shi, C. & Zhu, T. (2022) Pre-processing, quality assurance, and use of global atmospheric motion vector observations in CRA. *Journal of Meteorological Research*, 36(6), 947–962. Available from: <https://doi.org/10.1007/s13351-022-2041-2>
- Xu, J., Holmlund, K., Zhang, Q. & Schmetz, J. (2002) Comparison of two schemes for derivation of atmospheric motion vectors. *Journal of Geophysical Research*, 107, D144196. Available from: <https://doi.org/10.1029/2001JD000744>
- Zhang, L., Liu, Y., Liu, Y., Gong, J., Lu, H., Jin, Z. et al. (2019) The operational global four-dimensional variational data assimilation system at the China Meteorological Administration. *Quarterly Journal of the Royal Meteorological Society*, 145, 1882–1896. Available from: <https://doi.org/10.1002/qj.3533>
- Zou, X. & Zeng, Z. (2006) A quality control procedure for GPS radio occultation data. *Journal of Geophysical Research*, 111, D02112. Available from: <https://doi.org/10.1029/2005JD005846>

**How to cite this article:** Wang, J., Feng, J., Yang, Y., Hu, J. & Yang, J. (2025) A comprehensive quality control algorithm for atmospheric motion vectors and its impacts on analysis and forecast of the China Meteorological Administration Global Forecast System. *Quarterly Journal of the Royal Meteorological Society*, 151:e4960. Available from: <https://doi.org/10.1002/qj.4960>